A narrow Hα + [N II] filter for SITELLE: low-cost sustainable astronomical instrumentation for new compelling science cases at CFHT

Benoit Epinat[1, 2], Philippe Amram[2], Christophe Adami[2], Samuel Boissier[2], Alessandro Boselli[2], Delphine Russeil[2], Annie Zavagno[2], Anne-Laure Melchior[3], Laurent Drissen[4], and Gilles Joncas[4]

[1]Canada-France-Hawaii Telescope, Kamuela, HI, USA
[2]Aix Marseille Univ, CNRS, CNES, LAM, Marseille, France
[3]LERMA, UMR 8112, Observatoire de Paris & Sorbonne Université
[4]Université Laval, Québec (QC), Canada

September 2023

1 Project objectives and schedule

We propose to purchase a 13.5 k$ narrow-band filter for the imaging Fourier Transform Spectrometer (iFTS) SITELLE (a wide integral field spectrograph) at CFHT in order to open new scientific opportunities with this unique instrument. This filter will increase by a factor of about two both its spectral resolution and sensitivity, and will allow the exploration of prime interest science cases in various domains that are currently not within the reach of SITELLE. With a relatively low cost and few technical developments, this project will be an example of a sustainable astronomical project on the Mauna Kea sacred mountain that will benefit a broad community. It will enable French, Canadian and Hawaiian astronomers to tackle such science cases within reasonable exposure times on a 4-meter class telescope, much more adapted than IFUs on larger telescopes with small fields and lower spectral resolution, and with a much easier access. The funding will be shared between France and Canadian institutes and CFHT.

If this project is funded, we plan to order the filter in December 2023. With delays of 8 to 10 weeks for manufacturing, we will be able to have it on sky during semester 24A which starts in February 2024. During this semester, we will use engineering, commissioning and science verification time, to obtain first technical and science verification results by the end of the semester. This verification will include performance evaluation in terms of background level, gain in operation overheads and scheduling flexibility, as well as assessing the scientific accuracy based on previously observed fields (e.g. galaxy dynamics and line ratios, ram pressure stripping tails) and a test on more tricky observations (e.g. intermediate redshift cluster). This will allow the filter to be proposed to the whole CFHT community for two years, starting 25A, when a call for Large Programs proposal is foreseen.

2 Detailed scientific and technical justification

2.1 Galactic science

In gas rich galaxies, the emission lines from ionized nebulae are used to determine chemical abundances or identify processes (e.g. photoionization vs shocks) in the ISM. For example, H II regions are major data providers for research on the chemical evolution of galaxies. There are large uncertainties however in abundance determination due to our incomplete understanding of the physics of these nebulae being the sites of a significant number

of different processes: (1) complex chemistry at the interface with the parent molecular cloud, (2) large-scale gas flows away from the molecular cloud due to the pressure difference with the inter-cloud medium perturbed by stellar winds from the massive stars and jets from less massive stars resulting in a complex kinematics of colliding gas flows reaching supersonic speeds, (3) flow induced turbulence becoming a major player and (4) ill-understood microphysics. Expanding on the latter, the ionic abundances obtained from collisional excited lines (CELs) are 1.3 to 2.8 times smaller than those derived from optical recombination lines (ORLs) for H II regions (García-Rojas & Esteban 2007). Being even higher for Planetary Nebulae (Daigle et al. 2007; McNabb et al. 2013), this situation is called the Abundance Discrepancy Problem. The following projects bring support to SIGNAL, a 50-night CFHT large program of galaxy observations with SITELLE.

2.1.1 Feedback of massive stars on Galactic H II regions

Massive stars have a profound impact on their surrounding medium via radiative and mechanical feedback from their UV radiation and winds. They can alter the potential of molecular gas to form future generation of stars (negative feedback) by dispersing their parental molecular cloud (Walch et al. 2012) or inversely, as illustrated by figure 4 in Deharveng et al. (2010), they can promote (positive feedback) and trigger star formation while sweeping up gas into dense shells and by compressing pre-existing local density enhancement such as pillars or globules, as observed in the famous pillars of creation by the Hubble (Hester et al. 1996) and James Webb[1] space telescopes.

The development of infrared observatories allows to study the photodissociation region (PDR), which delineates the boundary between the H II region and the molecular interstellar medium, in great details in particular with the JWST (Berné et al. 2022). Well seen from their emission at 8 microns on Spitzer images, the PDR kinematics is now available from their [CII] 158 microns lines (e.g. Beuther et al. 2022) showing that bubble-like expanding morphologies are recurring structures in PDRs, that often wind-driving by the central stars is needed and that both positive and negative feedback can occur as a result of the expansion of H II regions. However, a clear description of the physical mechanisms that drive the feedback from high-mass stars is still missing. In this field, optical lines are key diagnostics to characterize the H II regions, their interface with the PDR and the feedback mechanisms. The importance to clarify the physical parameters of the ionized-molecular interface can be illustrated by the study of the tip of the pillars in NGC 6357 (Westmoquette et al. 2010), Carina (McLeod et al. 2016) and M16 (Flagey et al. 2020). In parallel, there are new evidence that the ionising radiation leaks througth the PDR (Luisi et al. 2016).

Because line widths represent the velocity dispersion along the line of sight which trace the physical processes (turbulence and gas flows) involved inside the H II regions and at their interface with the PDR (Barriault & Joncas 2007), Hα and [N II] lines are prominent lines which can be used to progress on our understanding of feedback from high-mass stars. The [NII] line is specially strong and very contrasted with respect to Hα in ionization fronts (Royer, M. & Joncas, G. 2023 MNRAS, submitted) making extremely useful to observe at high spectral resolution. To probe H II regions extension up to the PDR requires to reach typical surface brightness of 2 10 ^{16} erg s ^{1} cm ^{2} arcsec ^{2} and to follow the line width (and profile's shape) and velocity variation across the region requires at least a resolution of $R = 10000$.

SITELLE, with its large FOV and with a gain in e ciency and in spectral resolution (R = 10000) with the new filter, will be ideal to produce dispersion maps of a relatively large sample of well resolved H II regions in order to understand how the ionized gas interacts with the molecular gas at the PDR (< 1 pc) scale.

2.1.2 Planetary Nebulae and Wolf-Rayet stars: understanding the late stage of stellar evolution

PN and WR represent the late stage of the stars. Their importance in terms of chemical enrichment of the Galaxy is well known. From a general point of view these nebulae are formed by the current wind from the star blowing bubble into the ambient ISM and interacting also with the previous ejected envelop. As the gas forming these nebulae is the debris ejected by the progenitor star, the abundances of chemical elements in that gas which are not synthesized by the star provide information about the composition of the interstellar medium at the time of star formation. For example, in PNe, the [N II]λ6583 line may in some cases be 4-6 times stronger than the Hα line,

[1] https://www.esa.int/Science_Exploration/Space_Science/Webb/Webb_takes_a_stunning_star-filled_portrait_of_the_Pillars_of_Creation

while some can be hydrogen deficient objects (e.g. Schwarz et al. 1992). In this way, the optical line profiles across the region would help to better understand interactions between the different ejection phases, to probe their interaction with the ISM as well as to study the nebular physical conditions and abundance. In parallel, it is well known that PNe display morphologies encompassing elliptical, bipolar, multipolar, point-symmetric, multiple-shell and round shapes. The origin of this variety is still an area of research, involving stellar evolution, binarity, gas dynamics and nebular astrophysics. Also, in the ejecta, sub-structures emitting prominently in the [N II]λ6583 are noted in PNe (Balick 1987). They tend to occur along the nebula's symmetry axis. The origin of these structures is not clear even if Balick et al. (2020) and García-Segura et al. (2020) suggest that they can be explained as the remnants of slow, dense, collimated jets shaped by a toroidal magnetic field manifesting as shocked gas at the tips of the jets. As underlined in Kwitter & Henry (2022) the physics of the PN is still a hot topic and can be well probed from optical emission lines. **To conclude, 2D multiwavelength optical mapping of PN and WR is essential to better understand them. In this frame SITELLE is well suited to led such study and any improvement in the observation e ciency and resolution in the Hα-[N II]λ6583 domain is welcome.**

2.2 Extragalactic science: the local Universe

2.2.1 Stripped gas of interacting systems in the Virgo cluster

Galaxies located in high-density regions are subjects to different perturbing mechanisms able to drastically modify their evolution. They can be perturbed by the gravitational interaction with nearby companions in binary systems, in loose and compact groups, or in rich clusters of galaxies (tidal interactions). In the richest structures the gravitational perturbation induced by the multiple fly-by encounters with the other cluster members is combined with that of the gravitational potential well of the cluster itself. In these regions, galaxies moving at high velocity (1000 km/s) within the hot and dense ICM are also subject to the dynamical pressure exerted on their ISM while crossing the cluster (ram pressure; e.g. Boselli & Gavazzi 2006). All these mechanisms can efficiently remove some, if not most, of the galaxy ISM, thus quenching the activity of star formation on relatively short timescales. Star-forming spiral discs can thus be transformed in early-type systems and thus explain the dominant population observed in nearby clusters (morphology segregation effect, Dressler 1980).

If the nature of the stripping process is now fairly understood (e.g. Boselli et al. 2022), it is still unclear which is the fate of the stripped material. Observations and simulations consistently indicate that, although all gas phases can be perturbed, the dominant component of the ISM removed is the cold atomic hydrogen since the one less bound to the gravitational potential well of the galaxy. Once mixed with the hot ICM, it gets ionised becoming observable in the Balmer recombination lines. Indeed, prominent filaments and tails of ionised gas have been recently observed in the Virgo cluster thanks to the Hα narrow-band imaging survey of the cluster carried out at the CFHT (Boselli et al. 2018, VESTIGE). Most of these tails, which might extend on the plane of the sky up to more than 30', are associated to spiral galaxies (e.g. NGC 4569, Boselli et al. 2016). Others are far from any gas-rich systems and might thus be of different nature (Sun et al., in prep.).

IFU spectroscopy at high spectral resolution ($R > 3000$) on a large field as the one provided by SITELLE is of paramount importance for the study of these extended and low-surface brightness ($\Sigma(H\alpha)$ ' 5 10 ^{18} erg s ^{1} cm ^{2} arcsec ^{2}) features. The measurement of a well defined velocity gradient linking it to a parent galaxy is of primordial importance for identifying its origin. This exercise has been done up to now only in NGC 4569 and has required several observing runs at different facilities (APO telescope with a long-slit spectrograph; MMT with HECTOSPEC spectrograph; Sun et al. in prep) to cover the very extended ionised gas tail. The increased sensitivity of SITELLE with the proposed filter, coupled with its large FoV, will allow to cover the same region of the sky with just a few pointings, thus significantly increasing the efficiency in detecting these features. We will also detect at the same time the Hα and [N II]$\lambda\lambda$6548,6583 lines, and thus estimate an ionisation rate via the [N II]/Hα ratio, fundamental for constraining the gas phase transformation claimed by the tuned simulations that our and other teams are developing. The observations in the tail of NGC 4569, indeed, show an increase of the [N II]/Hα ratio with the distance from the galaxy, corroborating the picture where the gas is stripped as cold hydrogen and once mixed with the surrounding hot ICM becomes first ionised then hot. If this picture is confirmed, gas stripping of the recently infalling galaxies can contribute to the formation and pollution of the ICM emitting in X-rays, providing thus a different origin than the claimed ejecta via supernovae feedback of early-type galaxies during the first formation of clusters.

2.2.2 Kinematic properties of H ii regions in Virgo cluster galaxies

The perturbations induced by the hostile cluster environment can also drastically alter the activity of star formation of galaxies. The analysis of a large statistical sample of star forming systems in the Virgo cluster (Boselli et al. 2020) or of individual objects with a large set of multifrequency data (Boselli et al. 2021) has revealed that the external perturbations act down to scales of individual H ii regions. The activity is stopped in the outer disc, where star forming regions are totally lacking. In interacting systems, the gas is compressed at the interface of the cold galaxy ISM and the hot surrounding ICM, producing the most active star forming regions responsible for the enhanced activity observed in some of these perturbed objects. These bright H ii regions are formed on the leading side of the interaction, while tails of stripped gas with weak H ii regions are observed in the opposite direction. The formation of these H ii regions is due to a dynamical process between the cold ISM and the hot ICM and depends on the density of the two gas phases and on their relative velocity. The external pressure of the ICM is balanced by that of the galaxy ISM, which at the leading interface of the two media strongly depends on the expansion of the newly formed giant H ii regions. The study of the star formation process in these extreme environments and its accurate modelisation for tuned high resolution hydrodynamic simulations thus requires kinematic data.

With the proposed filter, SITELLE can provide high spectral resolution ($R > (10000)$ data cubes on a large FoV necessary to study the kinematics of individual H ii regions in perturbed galaxies located in the Virgo cluster. At this spectral resolution (10 km s^{-1} at H) the ionized gas kinematics are resolved in individual H ii regions. Thanks to the exquisite angular resolution of the CFHT, the same H ii regions are also spatially-resolved at the distance of the Virgo cluster (16.5 Mpc, where 1 arcsec = 80 pc). Their luminosity (L(H) 10^{36} erg s^{-1}) makes them ideal candidates for SITELLE for studying the kinematical properties of the huge number of H ii regions (100000) recently detected during the VESTIGE survey.

2.2.3 Exploration of nearby galaxies like M31

Andromeda is a typical green-valley galaxy, with a very little amount of gas in its central kiloparsec. The ionised gas in the central regions of M31 has been mapped by Ciardullo et al. (1988), who produced the highest S/N ratio map of H +[N ii] based on the compilation of a five-year nova survey published so far. This arc feature corresponds to the south-west part of the ring detected with Spitzer-IRAC data. Rubin & Ford (1971) measured that in this area [N ii] is three times stronger than H , which supports the shock hypothesis. It exhibits a turbulent spiral, which appears more face-on than does the main disc, lying in a disc, warped in a way that the gas south of the nucleus is viewed closer to face-on than the gas in the northern half of the galaxy. Boulesteix et al. (1987) observed this same area with a Fabry-Perot spectrograph to map the velocity field, and produced an [N ii] map which exhibits different patterns compared with the H +[N ii] one indicating that the gas does not have the same [N ii] ratio everywhere. The velocity field exhibits an irregular disc in rotation, with obvious perturbations along the minor axis which are interpreted as counter-rotations Saglia et al. (2010). It is difficult to understand the discrepancies observed in the ionised gas velocity field. The various lines might have different relative ratios from one region to another and might be affected differently by extinction. Additionally, it is possible that the ionised gas, like the molecular gas, exhibits several velocity components, and it has been not explored so far, but by Boulesteix et al. (1987), who mentioned line splittings greater than 30 km s^{-1} in the central region.

The sensitivity of SITELLE to detect ionised gas enabled to achieve a map at unprecedented depth (Figure 2) with the SN3 filter (at $R = 5000$), after the pioneering work of Boulesteix et al. (1987). However, the large stellar continuum due to the bulge is a limitation that could be overcome with a narrower filter, enabling a decrease of the continuum background associated to the bulge light, and an increase of the resolution and observing efficiency. Given the weakness of the lines, a better sensitivity will help to better subtract the H band seen in absorption and the atmospheric line present close to the emission line ($v = 0$), and to detect the multiple components present here. (1) Recent works show traces of recent AGN activity in an overall quiet region (Zhang et al. 2019; Alig et al. 2023). The presence of the very large stellar continuum next to the black hole (mag 13-14) has strongly limited our sensitivity in the circumnuclear region (100 pc). (2) In the whole 1-kpc central region (SITELLE's field), a better decomposition of the multiple kinematic components present in this region (e.g. Melchior & Combes 2011) will improve the excitation diagram of the region and help to disentangle shocks possibly due to the AGN from post-AGB excitation.

2.2.4 Other science cases

Several other extragalactic science cases could bene t from such a narrow-band lter, among which we can cite

- the physics of di use ionized gas (DIG) within nearby galaxies,
- the study of low surface brightness (LSB) galaxies.

Both would need the best sensitivity as possible and do not require to observe at [S ii] where LSB may be too faint.

2.3 Extragalactic science: intermediate redshift Universe

2.3.1 Galaxy pre-processing across the COSMIC web at intermediate redshift

Many studies have unambiguously shown that galaxy properties strongly depend on their small and large-scale environment. Most speci cally, clusters of galaxies have a well de ned red sequence and a large fraction of quiescent galaxies. These galaxies may result from various mechanisms at play in dense environments such as galaxy-galaxy dynamical interactions and mergers, dynamical interactions between galaxies and their large-scale environment inducing tidal stripping, interactions between cold gas within galaxies and hot intra-group/cluster medium (ram-pressure stripping), etc (e.g. Boselli & Gavazzi 2006). The fraction of quiescent galaxies and the fraction of massive star-forming galaxies increase when environment gets denser (e.g. Dressler 1980; Peng et al. 2010), which seems to indicate that the red sequence gradually forms as environments gets denser. Recently it has been proposed that is due to pre-processing that may occur while galaxies migrate from low- to high-density regions of the cosmic web (voids, walls, laments, groups, and clusters; e.g. De Lucia et al. 2012; Kraljic et al. 2018). This pre-processing may start at intermediate to high redshifts, when structures start to form and star-formation is still high. Identifying laments, groups and clusters requires extensive spectroscopic campaigns, most of the time using multi-object spectrographs and relying on pre-selection criteria based on magnitudes or stellar mass proxies. Another possibility is to study photometric redshift distributions, or to use narrow band imaging, but those need at some point to be con rmed spectroscopically, in particular to determine structures properties from the measurements of galaxies velocities. To go further, internal dynamics of galaxies is necessary to study the impact of environment on scaling relations and mass assemble (e.g. Mercier et al. 2022, 2023), but also to assess the spin orientation of galaxies with respect to laments and groups (e.g. Codis et al. 2018; Kraljic et al. 2021). The large FoV of SITELLE and its spectroscopic capabilities make it an ideal instrument to get all this information in one shot.

So far, galaxy clusters are the most studied structures, but what currently lacks is a variety of environments. We propose here to use SITELLE to observe clusters of galaxies at intermediate redshifts and their surroundings taking advantage of the NGVS and VESTIGE CFHT large programs. SITELLE already proved to be a powerful redshift machine by observing the Hin z 0:25 clusters (Liu et al. 2021) and we want to further use SITELLE with a higher sensitivity and spectral resolution to (i) asses the membership of galaxies large-scale structures (clusters, groups and laments), (ii) infer their environment (overdensity) and structure properties, and (iii) study the dynamical properties of galaxies in clusters and their surroundings. The new lter will cover a velocity range of $_V$ 4000 km s^{-1}, which is about four times larger as the typical velocity dispersion of massive clusters (1000 km s^{-1}), whereas the 11' SITELLE eld-of-view corresponds to more than 3 Mpc at 0:31 0:35, which allows one to observe galaxies up to about twice the typical Virial radius of massive clusters (1 Mpc). A handful of candidates are selected based on the NGVS background cluster catalog (Licitra et al. 2016), further con rmed thanks to the detection of ionized gas emission lines from background galaxies in the VESTIGE H narrow-band images (Boselli et al. 2018), and to the photometric redshifts of those galaxies (Raichoor et al. 2014). Line emitters are either seen in [O iii] 5007 at z 0:31, [O iii] 4959 at z 0:32, H 4861 at z 0:35, [O ii] 3727,3729 at z 0:76, or in Ly 1216 at z 4:40. The spectral resolution of SITELLE will allow us to disentangle the [O ii] doublet and the asymmetric Ly line from H and [O iii]. The NGVSLens photometric catalog (Raichoor et al. 2014) will be further used to asses galaxy properties. We expect several tens of spatially-resolved galaxies in each of the best three candidates at z 0:31 and 0:35 with a emission line surface brightness above 5 10 ^{17} erg s^{-1} cm^{-2} arcsec^{-2} over areas larger than one to ten square arcseconds (5 kpc to 20 kpc diameter).

3 Technical justification of the filter design

The filter we plan to purchase is very similar to the MegaCam filter, that has a transmission better than 90% between 6544Å < < 6632Å (see Fig. 2, left). This filter will cover both the H line and the [N ii] doublet, but not the [S ii] 6716,6731 doublet, that is either too faint or not necessary in many science cases. Its wavelength range is about four times narrower than that of the current SN3 SITELLE. In the following, we assume that noise is background dominated, which is the case under usual observing conditions with the actual SITELLE filters, and that emission lines are not resolved. In such conditions, in an iFTS, the signal is proportional to $T F$, T being the total exposure time and F the integrated line flux, whereas the variance is proportional to $T B$, where B is the background level (per unit wavelength) and is the wavelength bandwidth, so that the signal-to-noise ratio is proportional to $SNR / F \sqrt{T/(B)}$ (Maillard 1988). On the one hand, for a fixed total exposure time T, the new filter will reduce the noise contribution by a factor two with respect to SN3 (four times smaller) for target with faint emission lines, assuming a constant background (B sky and source continuum), since the signal from faint emission lines will not dominate the noise budget. It will result that the limiting emission line surface brightness S of objects within the reach of SITELLE will decrease by a factor of two. At fixed SNR, this translates into exposures four times shorter. On the other hand, narrowing the spectral range of the filter also decreases the number of scanning steps needed to reach a given spectral resolution. Because SITELLE is an off-axis iFTS, the gain for the proposed filter with respect to SN3 is a factor two to get the proper spectral coverage over the full FoV. This is due to the need to avoid aliasing at every position within the FoV (see Charlebois Master thesis, 2008). In theory, if objects do not extend over the whole FoV, we can further reduce the number of steps (and overheads) and reach a factor 4. Only about 840 (250) scanning steps will be necessary to obtain a spectral resolution of $R = 10000$ (3000), whereas SN3 would need 1680 (500) steps, which represents a non negligible gain of 50 (15) minutes overheads. A maximum spectral resolution of $R = 15000$ can be reached with the proposed filter.

We underline here that both the gains in SNR and spectral resolution can be obtained simultaneously. The saved overheads can also be used to increase the depth of observations at a given spectral resolution. We have made rough estimates using the SITELLE Exposure Time Calculator (https://etc.cfht.hawaii.edu/sit/) to infer a limiting surface brightness at 3 per pixel of 5×10^{-17} erg s^{-1} cm^{-2} arcsec^{-2} for unresolved emission lines within on-source exposures of 5h20m, under dark conditions and low airmass (1.2). Integrating the signal for extended sources over 3" (corresponding to 10×10 pixels), we might be able to obtain a limiting surface brightness at 3- of 5×10^{-18} erg s^{-1} cm^{-2} arcsec^{-2}. This is perfectly suited for the science cases developed above.

SITELLE filters are located in the f/8 beam, close to the telescope focal plane (Grandmont et al. 2012; Drissen et al. 2019). The effects of this configuration are illustrated in Fig. 2 (right) and are taken into account in the design of the new filter. In addition, we may expect central wavelength variations across the field. The main effect will be driven by filter manufacturing homogeneity defects. Specifications have been given to limit such variations by less than about 2 nm, similar to other SITELLE filters (Martin et al. 2021). We have checked that the proposed filter wavelength range contains enough sky lines to perform accurate calibration wavelength corrections. We have also ensured that SITELLE noise will remain in a background-dominated regime, in particular for faint sources for which the exposure time per step will be increased to reach unprecedented depths with SITELLE. Last, the larger steps needed to scan with a narrower filter will not increase the overheads that are dominated by detector readout time and mirror stabilisation that are equivalent and much larger than the displacement time.

References

Alig, C., Prieto, A., Blaña, M., et al. 2023, ApJ, 953, 109

Balick, B. 1987, AJ, 94, 671

Balick, B., Frank, A., & Liu, B. 2020, ApJ, 889, 13

Barriault, L. & Joncas, G. 2007, ApJ, 667, 257

Bernié, O., Habart, É., Peeters, E., et al. 2022, PASP, 134, 054301

Beuther, H., Schneider, N., Simon, R., et al. 2022, A&A, 659, A77

Boselli, A., Cuillandre, J. C., Fossati, M., et al. 2016, A&A, 587, A68

Boselli, A., Fossati, M., Ferrarese, L., et al. 2018, A&A, 614, A56

Boselli, A., Fossati, M., Longobardi, A., et al. 2020, A&A, 634, L1

Boselli, A., Fossati, M., & Sun, M. 2022, A&A Rev., 30, 3

Boselli, A. & Gavazzi, G. 2006, PASP, 118, 517

Boselli, A., Lupi, A., Epinat, B., et al. 2021, A&A, 646, A139

Boulesteix, J., Georgelin, Y. P., Lecoarer, E., Marcelin, M., & Monnet, G. 1987, A&A, 178, 91

Ciardullo, R., Rubin, V. C., Ford, W. Kent, J., Jacoby, G. H., & Ford, H. C. 1983, AJ, 88, 438

Codis, S., Jindal, A., Chisari, N. E., et al. 2018, Mon. Not. R. Astron. Soc., 481, 4753

Daigle, A., Joncas, G., & Parizeau, M. 2007, ApJ, 661, 285

De Lucia, G., Weinmann, S., Poggianti, B. M., Aragón-Salamanca, A., & Zaritsky, D. 2012, MNRAS, 423, 1277

Deharveng, L., Schuller, F., Anderson, L. D., et al. 2010, A&A, 523, A6

Dressler, A. 1980, ApJ, 236, 351

Drissen, L., Martin, T., Rousseau-Nepton, L., et al. 2019, MNRAS, 485, 3930

Flagey, N., McLeod, A. F., Aguilar, L., & Prunet, S. 2020, A&A, 635, A111

García-Rojas, J. & Esteban, C. 2007, ApJ, 670, 457

García-Segura, G., Taam, R. E., & Ricker, P. M. 2020, ApJ, 893, 150

Grandmont, F., Drissen, L., Mandar, J., Thibault, S., & Baril, M. 2012, in Society of Photo-Optical Instrumentation Engineers (SPIE) Conference Series, Vol. 8446, Ground-based and Airborne Instrumentation for Astronomy IV, ed. I. S. McLean, S. K. Ramsay, & H. Takami, 84460U

Hester, J. J., Scowen, P. A., Sankrit, R., et al. 1996, AJ, 111, 2349

Kraljic, K., Arnouts, S., Pichon, C., et al. 2018, MNRAS, 474, 547

Kraljic, K., Duckworth, C., Tojeiro, R., et al. 2021, MNRAS, 504, 4626

Kwitter, K. B. & Henry, R. B. C. 2022, PASP, 134, 022001

Licitra, R., Mei, S., Raichoor, A., et al. 2016, ApJ, 829, 44

Liu, Q., Yee, H. K. C., Drissen, L., et al. 2024, ApJ, 908, 228

Luisi, M., Anderson, L. D., Balser, D. S., Bania, T. M., & Wenger, T. V. 2016, ApJ, 824, 125

Maillard, J. P. 1988, in The Impact of Very High S/N Spectroscopy on Stellar Physics, ed. G. Cayrel de Strobel & M. Spite, Vol. 132, 71

Martin, T., Drissen, L., & Prunet, S. 2021, MNRAS, 505, 5514

McLeod, A. F., Gritschneder, M., Dale, J. E., et al. 2016, MNRAS, 462, 3537

McNabb, I. A., Fang, X., Liu, X. W., Bastin, R. J., & Storey, P. J. 2013, MNRAS, 428, 3443

Melchior, A. L. & Combes, F. 2011, A&A, 536, A52

Mercier, W., Epinat, B., Contini, T., et al. 2022, A&A, 665, A54

Mercier, W., Epinat, B., Contini, T., et al. 2023, arXiv e-prints, arXiv:2307.13355

Peng, Y.-j., Lilly, S. J., Kovač, K., et al. 2010, ApJ, 721, 193

Raichoor, A., Mei, S., Erben, T., et al. 2014, ApJ, 797, 102

Rubin, V. C. & Ford, W. Kent, J. 1971, ApJ, 170, 25

Saglia, R. P., Fabricius, M., Bender, R., et al. 2016, A&A, 509, A61

Schwarz, H. E., Corradi, R. L. M., & Melnick, J. 1992, A&AS, 96, 23

Walch, S. K., Whitworth, A. P., Bisbas, T., Wünsch, R., & Hubber, D. 2012, MNRAS, 427, 625

Westmoquette, M. S., Slavin, J. D., Smith, L. J., & Gallagher, J. S., I. 2010, MNRAS, 402, 152

Zhang, S., Wang, Q. D., Foster, A. R., et al. 2019, ApJ, 885, 157

Figure 1: Kinematics achieved with SN3 in M31's central eld (Cros et al. 2023, in prep.)The top panels display the intensity (left) and velocity eld (right) of this region with a weak gas content. The bottom panels display the velocity di erence of two components (left) when they are detected (probably due to shocks) and the velocity dispersion (right) derived from the Gaussian t on SITELLE sky-subtracted cube.

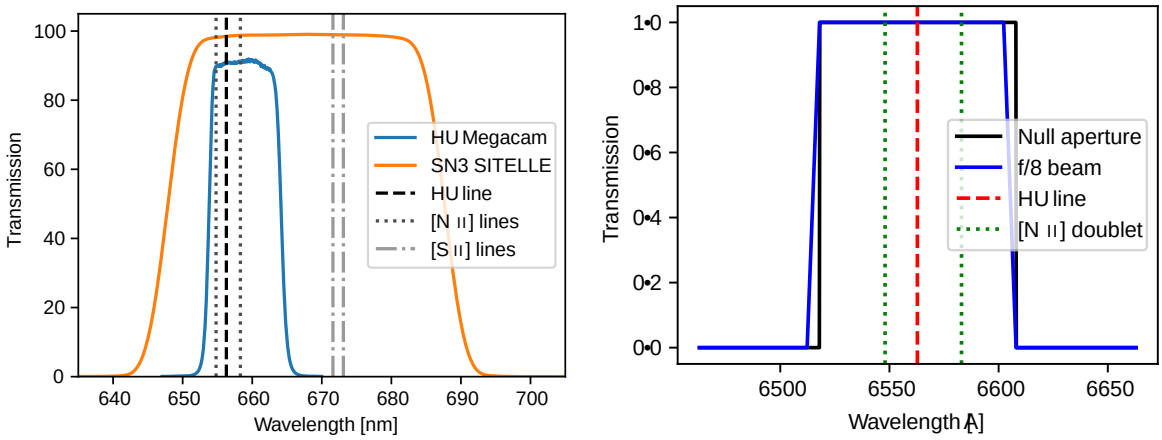

Figure 2: Left: the foreseen filter has similar specifications as the MegaCam Hα filter and is about four times narrower than the current SN3 SITELLE filter. Right: beam aperture blueshifts and broadens filter transmission. Rest-frame wavelengths of the main emission lines are shown as vertical lines.